Quantifying the Imprints of Stratospheric Contributions to Interhemispheric Differences in Tropospheric CFC-11, CFC-12, and N_2O Abundances

Megan Lickley[1] , Susan Solomon[1] , Doug Kinnison[2] , Paul Krummel[3] , Jens Mühle[4] , Simon O'Doherty[5] , Ronald Prinn[6] , Matthew Rigby[5] , Kane A. Stone[1] , Peidong Wang[1] , Ray Weiss[4] , and Dickon Young[5]

[1]Earth, Atmospheric, and Planetary Sciences, MIT, Cambridge, MA, USA, [2]Atmospheric Chemistry Observations and Modeling Laboratory, National Center for Atmospheric Research, Boulder, CO, USA, [3]Climate Science Centre, Oceans and Atmosphere, Commonwealth Scientific and Industrial Research Organization (CSIRO), Aspendale, VIC, Australia, [4]Scripps Institution of Oceanography, University of California San Diego, La Jolla, CA, USA, [5]School of Chemistry, University of Bristol, Bristol, UK, [6]Center for Global Change Science, Massachusetts Institute of Technology, Cambridge, MA, USA

Abstract For trace gases destroyed in the stratosphere, mass flux across the tropopause can substantially influence observed surface hemispheric differences (NH-SH). Here, we quantify associations between observed stratospheric and tropospheric NH-SH growth rate anomalies of CFC-11, CFC-12, and N_2O. We employ a chemistry climate model along with satellite and global surface station observations. Our model explains 60% of observed N_2O NH-SH growth rate variability from 2005 to 2019, compared to 30% for CFC-11% and 40% for CFC-12, supporting evidence that unexpected anthropogenic emissions caused sustained positive NH-SH anomalies in these CFCs from 2012 to 2017. Between 2012 and 2015, the observed CFC-11 NH-SH difference grew by 1.7 ppt; our model explains 0.5 ± 0.1 ppt of this growth, but not the duration. Our model suggests that in the absence of further emission anomalies, new NH-SH positive tracer anomalies should have occurred in 2020, and predicts small negative anomalies in 2021.

Plain Language Summary Changes in the North-South difference of surface trace gas abundances, denoted NH-SH, are often used as evidence of new emissions. However, atmospheric dynamics can also influence measurements of NH-SH. Importantly, anomalies in trace gas abundances in the stratosphere are transported down to the troposphere, influencing tropospheric NH-SH values. We quantify the stratospheric influence on NH-SH in models and observations for CFC-11, CFC-12, and N_2O. We provide a simple model to account for future stratospheric anomalies at the surface. Our model suggests that 60% of the variability in NH-SH can be explained by stratospheric anomalies. Following 2013, there was a sustained positive NH-SH anomaly in observations. Our results indicate that stratospheric influences can only partially explain this anomaly, supporting earlier work that an expected emission led to the observed positive NH-SH anomaly. This work shows that stratospheric observations improves interpretation of future emissions.

1. Introduction

Understanding global emissions of long-lived trace gases requires careful interpretation of in situ measurements. Emissions can be inferred from observed changes in atmospheric mole fractions along with an assumed atmospheric lifetime (WMO, 2003, 2018). However, sparse networks of in situ trace gas measurements together with large uncertainties in atmospheric lifetimes (Ko et al., 2013) can lead to large uncertainties in inferred emissions (Lickley, 2021). Experts have long looked to hemispheric differences in mole fractions of these chemicals as evidence to support conclusions about changes in anthropogenic emissions (Lovelock et al., 1973). However, recent work illustrates the importance of stratosphere - troposphere fluxes in driving anomalies of in situ trace gas measurements (Laube et al., 2020; Nevison et al., 2011; Ray et al., 2020; Ruiz et al., 2021). Ray et al. (2020) use modeling experiments to show that observed anomalies in North-South hemisphere differences (NH-SH) in CFC-11, CFC-12, and N_2O tropospheric mole fractions are associated with stratospheric anomalies driven by the Quasi Biennial Oscillation (QBO). This association has yet to be validated or quantified with stratospheric measurements, limiting our ability to interpret

short-term (i.e., year-long timescales) observed tropospheric NH-SH anomalies of these trace gases. Montzka et al. (2018), for example, pointed to positive NH-SH anomalies of CFC-11 after 2012 as evidence supporting unexpected CFC-11 emissions, while recognizing the potential for some stratospheric contribution.

Atmospheric sources of CFCs and N_2O are well documented (Prather et al., 2001, 2015). Their sources come from the surface through anthropogenic emissions and in the case of N_2O also through natural contribution (Prather et al., 2001, 2015), while destruction of these gases largely occurs in the tropical stratosphere through photolytic reactions (Douglass et al., 2008; Minschwaner et al., 2013). Destruction of these trace gases occurs in the stratosphere, and the Brewer Dobson circulation (Brewer, 1949; Dobson, 1956) transports air depleted in these trace gases into the troposphere at mid-to high latitudes. Mass transport across the extra-tropical tropopause varies with the annual cycle, with maximum descent occurring in each hemisphere's midwinter (Rosenlof, 1995) and NH late spring (Appenzeller et al., 1996). On interannual timescales, variability of mass flux across the tropopause is associated with the QBO, with enhanced meridional circulations, and thus enhanced downwelling in mid-to high latitudes, coinciding with the easterly phase of the QBO (see Baldwin et al. [2001] and references therein). Therefore, a contribution to interannual tropospheric trace gas anomalies due to stratospheric processes can be expected (as shown in Ray et al. [2020]).

While ongoing ground-level measurements of trace gases have been available for several decades, continuous stratospheric measurements of trace gases have only recently been made available through satellite-based monitoring experiments. In 2004, the Atmospheric Chemistry Experiment (ACE) satellite began measuring the atmospheric abundances of a range of trace gases (Bernath, 2017). Previous satellite missions measuring stratospheric trace gases have either ended within 10 years of their launch date (e.g., the Michelson Interferometer for Passive Atmospheric Sounding spectrometer on the Envisat mission; Fischer et al., 2008), or provide total column measurements of trace gases, rather than vertically resolved measurements (e.g., the Infrared Atmospheric Sounding Interferometer on MetOp-A; Hilton et al., 2012). The ACE satellite is now in its seventeenth year of operation, allowing for the novel quantification of the influence of stratospheric anomalies on tropospheric surface measurements for nearly two decades. This will aide in forecasting dynamically driven surface level anomalies months in advance. Another strength of the ACE instrument is its simultaneous observations of several trace gases.

In this paper we use regression analysis to relate stratospheric anomalies of CFC-11, CFC-12, and N_2O to tropospheric NH-SH anomalies using both a chemistry-climate model and observations. We first present results from a free-running ocean-atmosphere10-member ensemble of simulations from the Whole Atmospheric Chemistry Climate Model (WACCM). The model is nudged to a climatological averaged QBO to obtain repeatable QBO signatures. We use leave-one-out cross validation to test the suitability of regression modeling for predictive purposes using the suite of WACCM ensemble members. We then apply the predictive model to observations taken from ACE satellite stratospheric measurements together with the Advanced Global Atmospheric Gases Experiment (AGAGE) ground-level measurements. We show that our approach can quantify the amount of tropospheric variability in NH-SH tracer growth rates attributed to stratospheric variability, and we make a prediction for expected tropospheric NH-SH anomalies in 2021 in the absence of other sources and sinks.

2. Methods

2.1. Deriving the Predictive Model

To derive the parameters in the predictive model, we apply ordinary least squares to annual growth rates of our input variables to estimate β as follows;

$$\frac{d\left(NH_{trop,y} - SH_{trop,y}\right)}{dt} = \beta \frac{\mathrm{d}\left(NH_{\mathrm{strat,y-lag}}\right)}{dt} + \epsilon_y, \tag{1}$$

where the dependent variable, $d\left(NH_{trop,y} - SH_{trop,y}\right)/dt$, is the linearly detrended annual growth rates of the NH-SH gradient in the troposphere. The explanatory variable, $\mathrm{d}\left(NH_{\mathrm{strat,y-lag}}\right)/dt$, is the linearly detrended annual growth rates of the NH stratospheric mole fractions. We selected the NH as our explanatory variable (and did not include the SH) as the NH was shown to have higher correlations with surface level NH-SH values both in observations and WACCM. β and optimal lags between stratosphere and troposphere

are estimated separately for each of the ensemble members to achieve a sample mean and uncertainty of the model parameters; ϵ_y denotes error and is assumed to be normally distributed. Each hemispheric concentration average is computed taking the area weighted mean from 50° polewards. We tested various latitudinal extents for calculating hemispheric averages; extending to lower latitudes (e.g., 30° polewards) resulted in excessive smoothing of anomalies in lower altitudes while using higher latitudes (e.g., 70° polewards) led to seasonal gaps in ACE satellite data. Our choice of 50° polewards was a compromise between these two issues (see Figure S1). We note that the latitudes with the greatest impact on NH-SH need not occur where the largest absolute downward fluxes may occur, but are more likely to reflect where the difference between hemispheres maximizes. To compute the explanatory variable, $dNH_{strat,y-lag}$ / dt, we determine the height in the stratosphere where observed yearly NH growth rate anomalies are most strongly correlated with the surface level NH-SH growth rate anomalies. This occurs at ∼21 km as shown in Figures 2 and S2 for CFC-11 (similar results for CFC-12 and N_2O in Figures S8 and S9). The dependent variable is then computed using the modeled NH-SH difference at 8 km; surface mole fractions in WACCM are prescribed, therefore, NH-SH calculated at the surface would not reflect stratospheric transport. For each of the 10 ensemble members, we determine the initial lag times between 0 and 24 months that achieve the highest correlation between the explanatory and dependent variable, which is ∼11 ± 3 months. This means that it takes approximately 11 months for NH stratospheric anomalies to be observed in tropospheric NH-SH values.

One of the challenges in computing an unbiased estimator for β is that stratosphere–troposphere lag times vary over the time period of the simulation, with some years having faster stratosphere-troposphere exchange than others. This means anomalies between the stratosphere and troposphere do not always align at the same lagged interval. Varying lag times would also lead to a conservative estimate of correlations between the stratosphere and troposphere. Therefore, before computing β, we perform dynamic time warping (DTW) on the two timeseries to better align the anomalies in the regression analysis. DTW is an algorithm that allows comparison of two time series with varying speeds (Berndt & Clifford, 1994). The algorithm requires that the first and last elements in each time series align, and that mapping of elements from the initial timeseries to the adjusted timeseries occur monotonically in time. The algorithm searches for the optimal adjustment in the time variable to minimize the differences between the two timeseries. We add an additional constraint that adjustments of the initial lag cannot be larger than 3 months in either direction. An illustrative example of DTW is included in Figure S3. We only use model years from 2000 to 2025 in our regression analysis so that the coefficients are not affected by earlier years with high variability in modeled CFC emissions. After these lags are computed and imposed on the data, we compute β for each ensemble member. Our estimated predictive model parameters, β and lags, are shown in Table 1.

2.2. Model Validation

We test the WACCM-derived predictive model with a leave-one-out cross-validation (LOOCV) approach, wherein we derive the mean lag and β values from nine of the ensemble members and test its predictive power on the remaining ensemble member. Using LOOCV, R-squared and Root Mean Squared Error values of the predictive model using DTW are compared to a predictive model without a dynamically adjusted time series (noDTW). Results from LOOCV for CFC-11 are shown in Figure 1. Results for CFC-12 and N_2O are shown in Figures S4 and S5. The DTW model achieves an R-squared of 0.66 ± 0.13 for CFC-11 compared to 0.62 ± 0.11 for the noDTW model. Comparable R-squared values are achieved for CFC-12 and N_2O (see Table 1). As an example of the accuracy of the predictive mode, we show the leave-one-out prediction versus the simulated tropospheric NH-SH values in Figure 1d. For this member, the left-out sample (ensemble member 10) is within the 95% CI of the prediction throughout 78% of the time period. In other words, it falls outside of the 95% CI 22% of the time. The analogous predictions for all 10 members are shown in Figure S6.

2.3. Applying the Model to Observations

To apply the predictive model to observations of CFC-11, CFC-12, and N_2O, we follow the same approach for observations in computing the explanatory and dependent variables. As for the WACCM model output, both the explanatory and dependent variables are linearly detrended. We apply the mean of our sampled β parameters (shown in Table 1) and compute optimal lags between observed explanatory and dependent
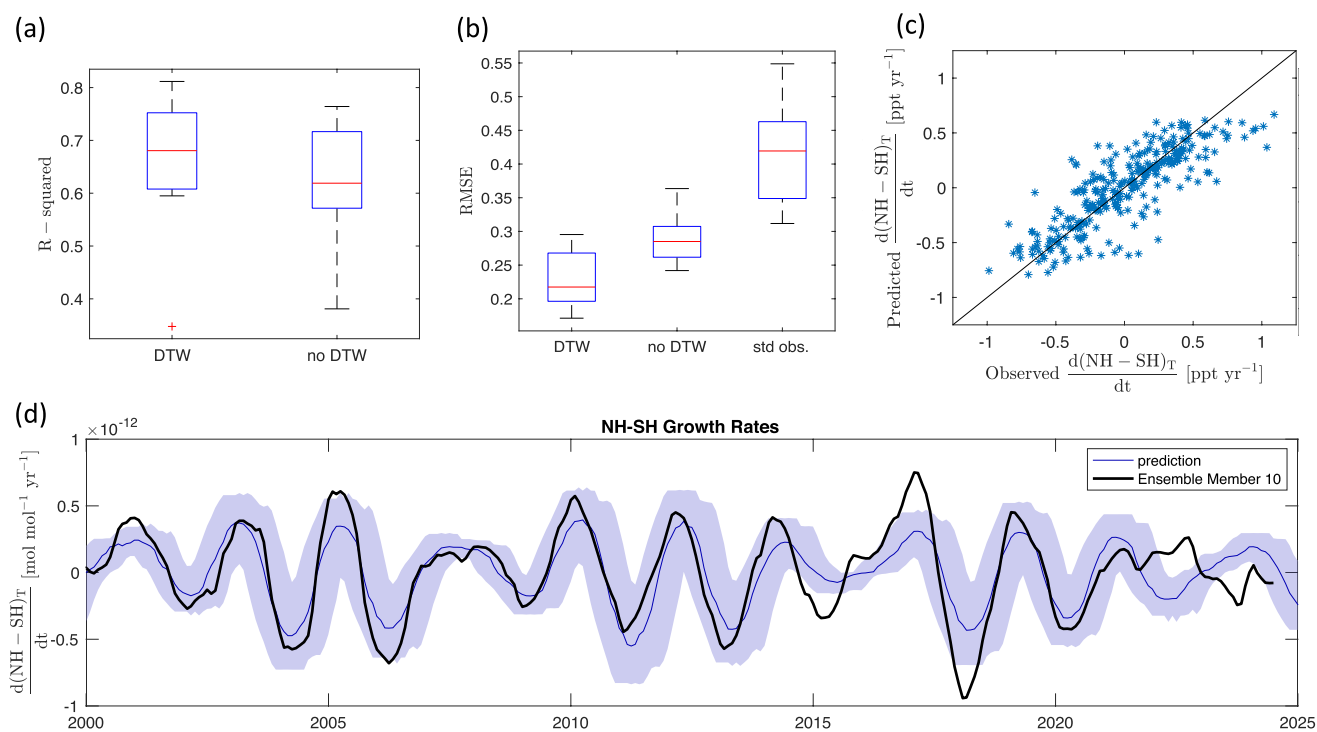
Figure 1. Leave-one-out cross-validation (LOOCV) for CFC-11 using the 10-member ensemble from WACCM. Regression parameters are calculated for nine of the ensemble members, and the mean of the parameters are applied to the remaining ensemble member's NH stratospheric detrended growth rates to provide a NH-SH tropospheric growth rate prediction. This is repeated for each ensemble members. (a) Boxplots of the 10 R-squared values from LOOCV, representing the fraction of NH-SH growth rate variability that can be explained by the predictive model. Results are shown for the dynamically time warped model (DTW) and the model without DTW (noDTW). Boxes indicate the interquartile range, red lines indicate median values and whiskers extend to the most extreme values within 1.5 times the interquartile range from the edge of the box. The red cross indicates outliers beyond the whisker lengths. (b) Boxplots of the root mean squared error (RMSE) using LOOCV. Results show box plots for RMSE for the DTW model, the noDTW model and standard deviations of observed tropospheric NH-SH detrended growth rates for comparison. (c) Yearly growth rate observations versus LOOCV predictions for the DTW model. A 1-1 line is provided for comparison (black). (d) Ensemble member 10s LOOCV predicted (blue) versus simulated (black) tropospheric NH-SH growth rate. The solid blue line is the median predicted value and the shaded region indicates the 95% CI.

variables. Uncertainties in predictions are estimated by sampling from the ensemble-derived β and lag parameters with $N = 1,000$.

3. Data

Satellite-based measurements come from the Atmospheric Chemistry Experiment (ACE) satellite mission (Bernath, 2017). Data are in the form of zonal averages (5° wide bands), at a 1 km vertical resolution, and are binned by season (March–May, June–August, September–November, December–February). Data are available from pole to pole, from March 2004 to August 2020, and from an altitude of 5.5–28.5 km (for CFC-11) to 35.5 km (for CFC-12) and to 95.5 km (for N_2O). Trace gas observations from the lower troposphere come from the AGAGE monitoring network (see Supporting Information; Prinn et al., 2018). To fill gaps during periods of instrumental down-time, monthly means are extracted from the AGAGE 12-box model, into which the AGAGE data has been assimilated (Rigby et al., 2013). Similar to Montzka et al. (2018) and Rigby et al. (2019), a least-squares inverse method is employed in which emissions are estimated using the data and the model without a prior constraint. The model is constrained by monthly mean baseline-filtered observations from January 1978 to December 2019, binned into semi-hemispheres (90°–30°S, 30°S–eq, eq–30°N, 30°–90°N, see Text S1 for details).

The predictive model is derived using a 10-member ensemble of simulations from a fully coupled atmosphere-ocean version of WACCM version 4 (Stone et al., 2018, 2020). The ensemble simulations are run from 1995 to 2025 following the CCMI REF-C2 scenario definition (Morgenstern et al., 2017). These simulations
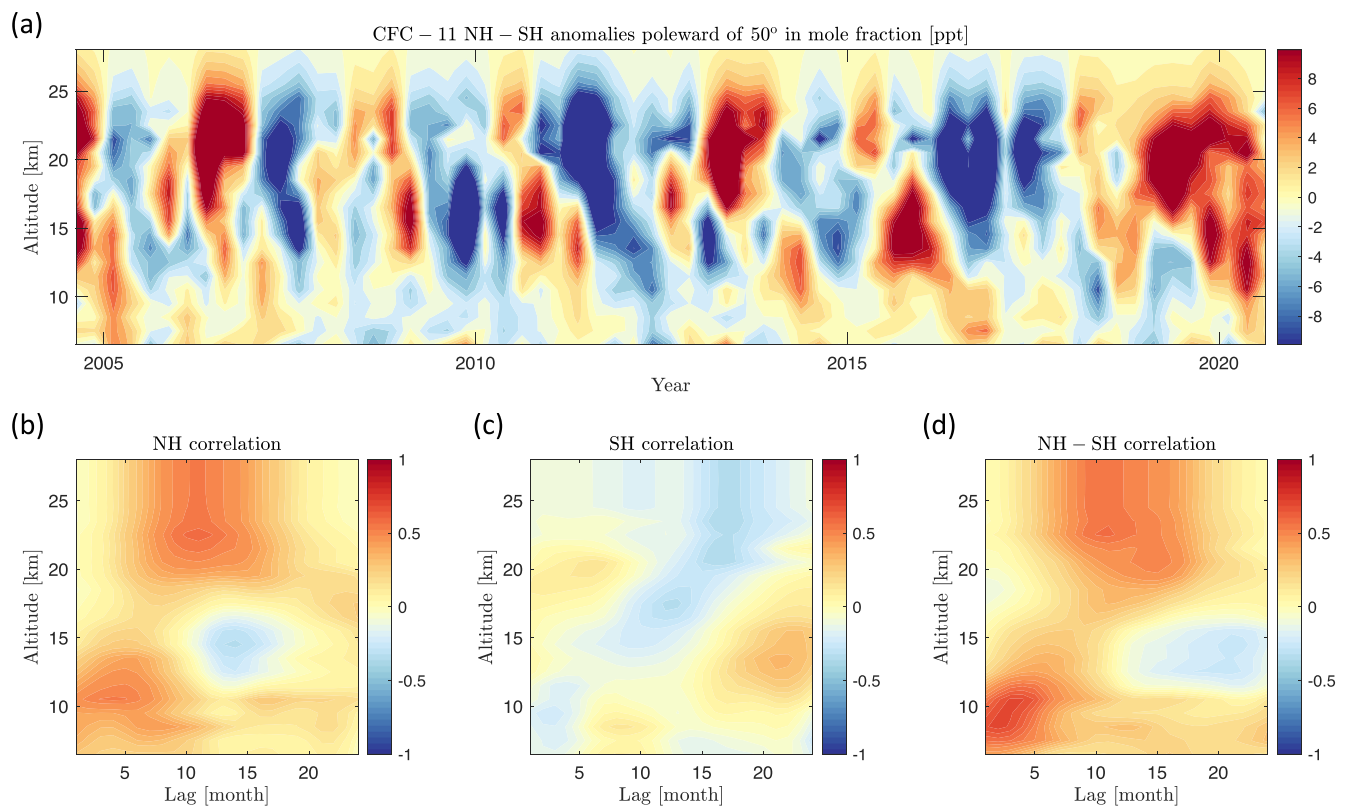
(a)

(b)   (c)   (d)

Figure 2. Observed CFC-11 concentration anomalies and correlations with surface measurements. (a) ACE derived North-South (NH-SH) CFC-11 anomalies, poleward of 50°. (b) Correlation coefficient between AGAGE surface NH-SH anomalies and ACE Northern Hemisphere anomalies (NH) poleward of 50°. (c) As in (b) but for the Southern Hemisphere (SH). (d) As in (b) but for NH-SH. Both ACE and AGAGE are de-seasonalized and detrended relative to a piece-wise linear trend, with a breakpoint occurring at 2012 (see main text).

have a repeated cyclic 28-months QBO, no 11-years solar cycle or solar energetic particle events. Initialization of the ensembles follows the approach in Solomon et al. (2017). In this scenario, mole fractions of ozone depleting substances follow the WMO (2011) A1 scenario (Daniel et al., 2011) and are based on observations from a variety of sources, including AGAGE, through 2009 (see Table 1.1 in WMO (2011) for

Table 1
Model Parameters and R-Squared Values for the Predictive Model Applied to WACCM Ensemble Members and Observations

	CFC-11	CFC-12	N_2O
Model parameters			
β	0.036 ± 0.007	0.013 ± 0.002	0.012 ± 0.004
Lag (months)	10.9 ± 2.8	11.7 ± 2.6	11.6 ± 2.6
Leave-one-out cross validation			
R^2 **(DTW)**	0.66 ± 0.13	0.72 ± 0.10	0.71 ± 0.10
R^2 **(noDTW)**	0.62 ± 0.11	0.60 ± 0.10	0.59 ± 0.10
Predictive model applied to observations			
R^2 **(noDTW)**	0.32	0.41	0.58

Note. Reported values indicate the mean and 1-sigma range from the 10 WACCM ensemble members. For ensemble members, R-squared is provided both for the dynamically time warped data (DTW), and the non DTW data (noDTW).

more details). The greenhouse gases (e.g., CO_2, N_2O, and CH_4) surface mole fractions, along with surface emissions of ozone and aerosol precursors are taken from Meinshausen et al. (2011). These prescribed surface forcings are based on observations through 2004; for the 2005–2025 period the RCP6.0 projection is used. See Figure S7 for WACCMs prescribed mole fractions of CFC-11, CFC-12 and N_2O. We consider monthly mole fractions at a 1.9° latitude × 2.5° longitude resolution from the surface up to 5.1×10^{-6} hPa (~140 km), with 66 vertical levels. The predictive model is derived using WACCM simulations instead of observations due to the limited timeframe of stratospheric observations. Further, this approach allows us to isolate the stratosphere influence on the troposphere as it does not require assumptions regarding recent unexpected emissions.

4. Results

Figure 2 illustrates the ACE observed CFC-11 NH-SH anomalies throughout the lower stratosphere and upper troposphere. Here, anomalies are calculated after de-seasonalizing and removing a piece-wise linear trend, with a breakpoint at 2012 (following Montzka et al. [2018]). The piece-wise trend was chosen so that anomalies reflect natural variability relative to a background trend that includes an unexpected emissions increase following 2012 (Montzka et al., 2018). The analogous figure for WACCM is shown in Figure S2. Note that the detrending and de-seasonalizing applied in Figure 2 is used only to illustrate the transportation of stratospheric anomalies apparent in ACE observations, and is not the approach taken in the predictive model (as described in the Methods). We note a discernable signal of NH-SH anomalies propagating down through the atmosphere. The same occurs for CFC-12 and N_2O (Figures S8 and S9). Strong correlations between trace gases have been found with ACE data, see for example, Brown et al. (2013). This supports the view that differences we see among gases are more likely to be a reflection of surface emissions than stratospheric phenomena.

Figure 2 also illustrates correlations of anomalies between ACE observations and AGAGE surface level observations; these are remarkably similar to those obtained in WACCM as shown in Figure S2. While observed NH-SH stratospheric anomalies appear strongly correlated to surface NH-SH anomalies in this figure, we chose to use NH stratospheric *growth rates* as our explanatory variable because that yielded higher correlations with surface growth rate anomalies in WACCM.

Figure 3 provides the central results of our study, focusing on CFC-11. CFC-12 and N_2O results are shown in Figures S10 and S11. Figures 3a and 3b show the timeseries of the yearly moving averages and growth rates in stratospheric and tropospheric observations, with anomalies in the troposphere lagging anomalies in the stratosphere by ~8 months. Interpreting the magnitude of NH-SH anomalies (shown in Figure 3c) for all trace gases depends on assumptions about the background trends both at the surface due to emissions, and in the stratosphere relating to atmospheric destruction and stratosphere-troposphere exchange. In this analysis we use an exponential function to approximate the background trends in both the stratosphere and troposphere using observations from 2000 to 2012. We then apply our model to predict tropospheric NH-SH values relative to the background NH-SH trend (see Supporting Information for details).

The NH-SH difference in the troposphere shows a clear and sustained departure from its trend around 2013 (Figures 3a and 3c). While recognizing the potential for some dynamical contribution, Montzka et al. (2018) concluded that observed positive NH-SH anomalies in CFC-11 at this time could not be explained by dynamical variability alone, indicating an increased and sustained anthropogenic emission was occurring in the northern hemisphere. This increased emission is commonly referred to as an unexpected emission, as the Montreal Protocol prohibits production of CFCs after 2010, globally. Our results quantify the stratospheric dynamics contribution to the observed time series (Figure 3d). A positive anomaly also occurs in the stratosphere ~8 months prior to the tropospheric positive anomaly after 2012. Importantly, the magnitude of this predicted anomaly originating in the stratosphere is about one third of the observed surface NH-SH anomaly (0.5 ± 0.1 ppt relative to 1.7 ppt between 2012 and 2015) and the duration in the stratosphere is short (~2 years) relative to the observed surface NH-SH anomaly (see Figure 3c). A smaller anomaly is also observed following 2012 for CFC-12 (0.2 ± 0.1 ppt) and N_2O (0.3 ± 0.1 ppb). In the absence of changes in surface level sources and sinks, our model predicts that a positive CFC-11 NH-SH anomaly of 0.5 ± 0.14 ppt would be expected during 2020, followed by a decrease in 2021 (−0.18 ± 0.12 ppt), due to stratospheric
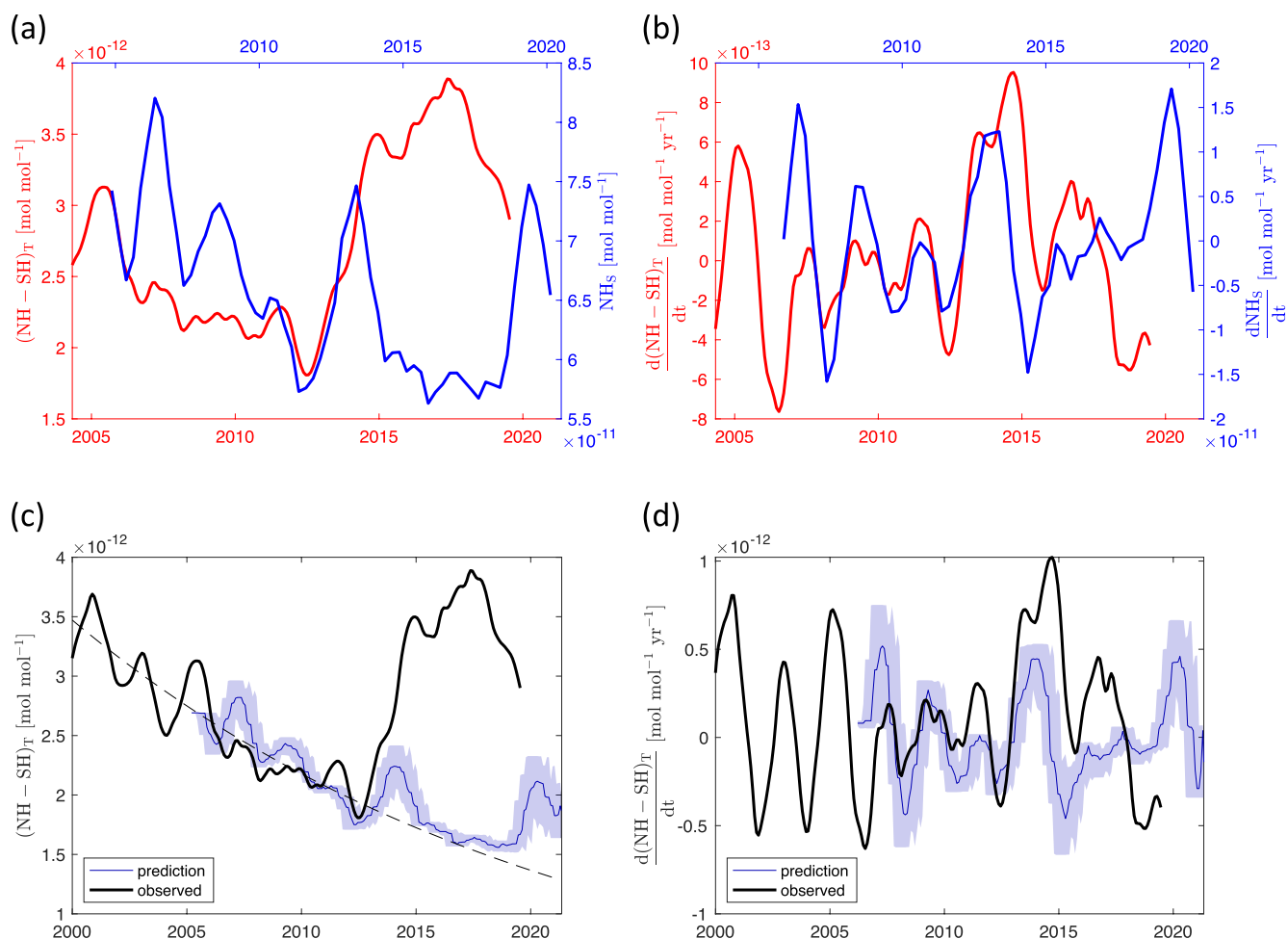
Figure 3. Observed and predicted NH-SH differences for CFC-11. (a) The yearly moving average of observed tropospheric NH-SH difference (denoted $(NH-SH)_T$, axis on the left in red) and stratospheric NH mole fractions (denoted NH_S, axis on right in blue). (b) The yearly moving average growth rates of tropospheric NH-SH differences and stratospheric NH mole fractions. The two time axes in (a) and (b) are adjusted by the mean lag times. (c) Observed versus predicted tropospheric NH-SH difference, where the prediction is relative to an assumed background trend (dashed line) and thus subject to large uncertainties. (d) Observed versus predicted linearly detrended tropospheric NH-SH growth rates. The blue line indicates the median sampled prediction and the shaded region indicates the 95% CI.

impacts on the troposphere (as shown in Figure 3c). We predict comparable 2020 anomalies for CFC-12 (0.3 ± 0.12 ppt) and N_2O (0.2 ± 0.07 ppb), and negative anomalies in 2021 for both CFC-12 (-0.3 ± 0.2 ppt) and N_2O (-0.16 ± 0.11) ppb. We note that the expected anomalies could be partially or even wholly offset by decreases in anthropogenic emissions over this time period (Montzka et al., 2021), but our results should help to interpret whatever changes in emissions do occur. From the WACCM simulations, we estimate anomalies last on average 1 ± 0.5 year from peak to trough, (95% CI of 0.1–2.3 years) suggesting that the sustained increase in the CFC-11 NH-SH difference after 2014 is virtually certain not to be due to stratospheric influences alone.

R-squared values from the leave-one-out cross-validation (shown in Table 1) indicate that, in the absence of significant changes in anthropogenic emissions, stratospheric anomalies can explain up to ~70% ± 10% of surface level NH-SH growth rate anomalies. If DTW is not applied to the data, our model would explain ~60% ± 10% of growth rate variability (shown in the noDTW case in Table 1). This is an important distinction—we do not perform DTW on observations to avoid the risk of over attributing surface anomalies to stratospheric anomalies, so we expect the R-squared of our predictive model applied to observations to be conservative. Our predictive model produces an R-squared of 0.3, 0.4, and 0.6 for CFC-11, CFC-12, and N_2O, respectively. For CFC-11 and CFC-12, this falls outside of the 1-sigma range of the noDTW R-squared values

derived from the WACCM validation, whereas the R-squared for N_2O is equal to the mean noDTW R-squared from the WACCM validation (see Table 1). This suggests that emission anomalies are likely less pronounced relative to stratospheric influences for N_2O compared to CFC-11 and CFC-12 over this time period. In other words, N_2O observations exhibit similar correlations between the stratosphere and troposphere as WACCM simulations, whereas CFC-11 and CFC-12 do not; we interpret this to support earlier work that identifies new and unexpected emissions of CFC-11 after 2012 (Montzka et al., 2018; Rigby et al., 2019), and also to a lesser extent for CFC-12 (Lickley et al., 2021; Park et al., 2021). We note, however, that decoupling between the stratospheric and tropospheric anomalies are less pronounced after 2012 for CFC-12 such that the present study cannot identify the timing and occurrence of anomalous CFC-12 emissions.

5. Conclusions

In this paper, we set out to derive a predictive model to estimate the contribution of stratospheric trace gas anomalies to surface NH-SH anomalies. We find strong correlations between stratospheric NH and tropospheric NH-SH growth rates in WACCM simulations for CFC-11, CFC-12, and N_2O, and our simple predictive model can explain up to 70% of modeled tropospheric NH-SH growth rate variability. Applying the predictive model to ACE satellite stratospheric observations and AGAGE in situ observations yields comparable results to WACCM simulations for N_2O and weaker results for CFC-11 and CFC-12. Most notably, the anomalous growth in the NH-SH differences observed after 2012 cannot be explained with our simple predictive model, supporting previous studies that other contributing factors (i.e., increased anthropogenic emissions) are at play.

Montzka et al. (2021) and Park et al. (2021) provide evidence for reduced global and eastern Chinese CFC-11 emissions (respectively) in 2019. Looking forward, our predictive model suggests that in the absence of further anomalous emissions, a new NH-SH positive anomaly should have occurred in 2020, and that negative anomalies can be expected in 2021. If, however, anthropogenic emissions continue to be reduced over this time period, this may serve to offset part of the positive anomaly descending from the stratosphere.

The work presented in this paper underscores the value of both stratospheric and surface global observations, and the need to account for stratospheric dynamics in interpreting surface level NH-SH anomalies in terms of anthropogenic impacts. Here, we provide a simple model to do so for CFC-11, CFC-12, and N_2O. We applied our analysis to NH-SH growth rates, as that required few assumptions regarding background trends relative to tropospheric average growth rates. Further analysis would be required to extend this work to absolute tropospheric averages, or other trace gases. Our results show that interpreting any future unexpected emissions and potential production outside the Montreal Protocol can benefit from stratospheric observations and analysis.

Data Availability Statement

All data used in this analysis can be freely obtained online (at https://doi.org/10.7910/DVN/JECPN8). All code is available upon request from M.L. (mlickley@mit.edu).

References

Appenzeller, C., Holton, J. R., & Rosenlof, K. H. (1996). Seasonal variation of mass transport across the tropopause. *Journal of Geophysical Research Atmospheres*, *101*(D10), 15071–15078. https://doi.org/10.1029/96JD00821

Baldwin, M. P., Gray, L. J., Dunkerton, T. J., Hamilton, K., Haynes, P. H., Holton, J. R., et al. (2001). The quasi-biennial oscillation. *Reviews of Geophysics*, *2*(39), 179–229. https://doi.org/10.1029/1999rg000073

Bernath, P. F. (2017). The atmospheric chemistry experiment (ACE). *Journal of Quantitative Spectroscopy and Radiative Transfer*, *186*, 3–16. https://doi.org/10.1016/j.jqsrt.2016.04.006

Berndt, D., & Clifford, J. (1994). Using dynamic time warping to find patterns in time series. In KDD Workshop (Vol. 10, 16, pp. 359–370). Retrieved from http://www.aaai.org/Papers/Workshops/1994/WS-94-03/WS94-03-031.pdf

Brewer, A. W. (1949). Evidence for a world circulation Provided by the measurements of helium and water vapor distribution in the Stratosphere. *Quarterly Journal of Royal Meteorological Society*, *75*, 351–363. https://doi.org/10.1002/qj.49707532603

Brown, A. T., Volk, C. M., Schoeberl, M. R., Boone, C. D., & Bernath, P. F. (2013). Stratospheric lifetimes of CFC-12, CCl_4, CH_4, CH_3Cl, and N_2O from measurements made by the Atmospheric Chemistry Experiment-Fourier transform spectrometer (ACE-FTS). *Atmospheric Chemistry and Physics*, *13*(14), 6921–6950.

Daniel, J. S., Velders, G. J. M., Morgenstern, O., Toohey, D. W., Wallington, T. J., Wuebbles, D. J., et al. (2011). A focus on information and options for policymakers. *Scientific assessment of ozone depletion*.

Dobson, G. M. B. (1956). Origin and distribution of the polyatomic molecules in the atmosphere. *Proceedings of the Royal Society of London - Series A: Mathematical and Physical Sciences*, *236*, 187–193. https://doi.org/10.1098/rspa.1956.0127

Douglass, A. R., Stolarski, R. S., Schoeberl, M. R., Jackman, C. H., Gupta, M. L., Newman, P. A., et al. (2008). Relationship of loss, mean age of air and the distribution of CFCs to stratospheric circulation and implications for atmospheric lifetimes. *Journal of Geophysical Research: Atmospheres*, *113*(14), 1–14. https://doi.org/10.1029/2007JD009575

Fischer, H., Birk, M., Blom, C., Carli, B., Carlotti, M., Von Clarmann, T., et al. (2008). MIPAS: An instrument for atmospheric and climate research. *Atmospheric Chemistry and Physics*, *8*(8), 2151–2188. https://doi.org/10.5194/acp-8-2151-2008

Hilton, F., Armante, R., August, T., Barnet, C., Bouchard, A., Camy-Peyret, C., et al. (2012). Hyperspectral earth observation from IASI. *Bulletin of the American Meteorological Society*, *93*(3), 347–370. https://doi.org/10.1175/BAMS-D-11-00027.1

Ko, M., Newman, P., Reimann, S., & Strahan, S. (2013). SPARC report on the lifetimes of stratospheric ozone-depleting substances, their replacements, and related species. *SPARC Report N. 6*, WCRP-15/2013.

Laube, J. C., Elvidge, E. C. L., Adcock, K. E., Baier, B., Brenninkmeijer, C. A. M., Chen, H., et al. (2020). Investigating stratospheric changes between 2009 and 2018 with halogenated trace gas data from aircraft, AirCores, and a global model focusing on CFC-11. *Atmospheric Chemistry and Physics*, *20*(16), 9771–9782. https://doi.org/10.5194/acp-20-9771-2020

Lickley, M. (2021). *Joint inference of CFC lifetimes and banks suggests previously unidentified emissions*. Zenodo. https://doi.org/10.5281/zenodo.4602326

Lickley, M., Fletcher, S., Rigby, M., & Solomon, S. (2021). Joint inference of CFC lifetimes and banks suggests previously unidentified emissions. *Nature Communications*, *12*(1), 1–10.

Lovelock, J. E., Maggs, R. J., & Wade, R. J. (1973). Halogenated hydrocarbons in and over the Atlantic. *Nature*, *241*(5386), 194–196. https://doi.org/10.1038/241194a0

Meinshausen, M., Smith, S. J., Calvin, K., Daniel, J. S., Kainuma, M. L. T., Lamarque, J., et al. (2011). The RCP greenhouse gas concentrations and their extensions from 1765 to 2300. *Climatic Change*, *109*(1), 213–241. https://doi.org/10.1007/s10584-011-0156-z

Minschwaner, K., Hoffmann, L., Brown, A., Riese, M., Müller, R., & Bernath, P. F. (2013). Stratospheric loss and atmospheric lifetimes of CFC-11 and CFC-12 derived from satellite observations. *Atmospheric Chemistry and Physics*, *13*(8), 4253–4263. https://doi.org/10.5194/acp-13-4253-2013

Montzka, S. A., Dutton, G. S., Portmann, R. W., Chipperfield, M. P., Davis, S., Feng, W., et al. (2021). A decline in global CFC-11 emissions during 2018-2019. *Nature*, *590*, 428–432. https://doi.org/10.1038/s41586-021-03260-5

Montzka, S. A., Dutton, G. S., Yu, P., Ray, E., Portmann, R. W., Daniel, J. S., et al. (2018). An unexpected and persistent increase in global emissions of ozone-depleting CFC-11. *Nature*, *557*(7705), 413–417. https://doi.org/10.1038/s41586-018-0106-2

Morgenstern, O., Hegglin, M., Rozanov, E., O'Connor, F., Luke Abraham, N., Akiyoshi, H., et al. (2017). Review of the global models used within phase 1 of the Chemistry-Climate Model Initiative (CCMI). *Geoscientific Model Development*, *10*(2), 639–671. https://doi.org/10.5194/gmd-10-639-2017

Nevison, C. D., Dlugokencky, E., Dutton, G., Elkins, J. W., Fraser, P., Hall, B., et al. (2011). Exploring causes of interannual variability in the seasonal cycles of tropospheric nitrous oxide. *Atmospheric Chemistry and Physics*, *11*(8), 3713–3730. https://doi.org/10.5194/acp-11-3713-2011

Park, S., Western, L. M., Saito, T., Redington, A. L., Henne, S., Fang, X., et al. (2021). A decline in emissions of CFC-11 and related chemicals from eastern China. *Nature*, *590*, 433–437. https://doi.org/10.1038/s41586-021-03277-w

Prather, M., Ehhalt, D., Dentener, F., Derwent, R., Dlugokencky, E., Holland, E., et al. (2001). Atmospheric chemistry and greenhouse gases. In J. T. Houghton, Y. Ding, D. J. Griggs, M. Noguer, P. J. van der Linden, X. Dai, et al. (Eds.), *Climate change 2001: Scientific basis: Contribution to Working Group I to the Third Assessment Report of the Intergovernmental Panel on Climate Change* (p. 881). Cambridge University Press.

Prather, M. J., Hsu, J., Deluca, N. M., Jackman, C. H., Oman, L. D., Douglass, A. R., et al. (2015). Measuring and modeling the lifetime of nitrous oxide including its variability. *Journal of Geophysical Research: Atmospheres*, *120*(11), 5693–5705. https://doi.org/10.1002/2015JD023267

Prinn, R. G., Weiss, R. F., Arduini, J., Arnold, T., Langley Dewitt, H., Fraser, P. J., et al. (2018). History of chemically and radiatively important atmospheric gases from the Advanced Global Atmospheric Gases Experiment (AGAGE). *Earth System Science Data*, *10*(2), 985–1018. https://doi.org/10.5194/essd-10-985-2018

Ray, E. A., Portmann, R. W., Yu, P., Daniel, J., Montzka, S. A., Dutton, G. S., et al. (2020). The influence of the stratospheric Quasi-Biennial Oscillation on trace gas levels at the Earth's surface. *Nature Geoscience*, *13*(1), 22–27. https://doi.org/10.1038/s41561-019-0507-3

Rigby, M., Park, S., Saito, T., Western, L. M., Redington, A. L., Fang, X., et al. (2019). Increase in CFC-11 emissions from eastern China based on atmospheric observations. *Nature*, *569*(7757), 546–550. https://doi.org/10.1038/s41586-019-1193-4

Rigby, M., Prinn, R. G., O'Doherty, S., Montzka, S. A., McCulloch, A., Harth, C. M., et al. (2013). Re-evaluation of the lifetimes of the major CFCs and CH_3 CCl_3 using atmospheric trends. *Atmospheric Chemistry and Physics*, *13*, 2691–2702. https://doi.org/10.5194/acp-13-2691-2013

Rosenlof, K. H. (1995). Seasonal cycle of the residual mean meridional circulation in the stratosphere. *Journal of Geophysical Research: Atmospheres*, *100*(D3), 5173–5191. https://doi.org/10.1029/94jd03122

Ruiz, D. J., Prather, M. J., Strahan, S. E., Thompson, R. L., Froidevaux, L., & Steenrod, S. D. (2021). How atmospheric chemistry and transport drive surface variability of N_2O and CFC-11. *Journal of Geophysical Research: Atmospheres*, *126*. https://doi.org/10.1029/2020jd033979

Solomon, S., Ivy, D., Gupta, M., Bandoro, J., Santer, B., Fu, Q., et al. (2017). Mirrored changes in Antarctic ozone and stratospheric temperature in the late 20th versus early 21st centuries. *Journal of Geophysical Research: Atmospheres*, *122*(16), 8940–8950. https://doi.org/10.1002/2017JD026719

Stone, K. A., Solomon, S., & Kinnison, D. E. (2018). On the identification of ozone recovery. *Geophysical Research Letters*, *45*(10), 5158–5165. https://doi.org/10.1029/2018GL077955

Stone, K. A., Solomon, S., & Kinnison, D. E. (2020). Prediction of northern hemisphere regional sea ice extent and snow depth using stratospheric ozone information. *Journal of Geophysical Research: Atmospheres*, *125*(22), 1–14. https://doi.org/10.1029/2019JD031770

WMO. (2003). *Scientific assessment of ozone depletion: 2002, global ozone research and monitoring project-report no. 47*. World Meteorological Organization (WMO).

WMO. (2011). *Scientific assessment of ozone depletion: 2010, global ozone research and monitoring project-report no. 52*. World Meteorological Organization (WMO).

WMO. (2018). *Scientific assessment of ozone depletion: 2018, global ozone research and monitoring project-report no. 58*. World Meteorological Organization (WMO).